Journal of the Korean Physical Society, Vol. 73, No. 7, October 2018, pp. 877∼882

Single-Photon-Emission Computed Tomography with Neutron Activation for Material Inspection

Taewoong Lee
Health Science Research Center, Korea University, Seoul 02841, Korea and
RI Applied Research Team, Korea Institute of Radiologic and Medical Sciences, Seoul 01812, Korea

Minho Kim
Division of Medical Radiation Equipment, Korea Institute of Radiologic and Medical Sciences, Seoul 01812, Korea and
Department of Bio-Convergence Engineering, Korea University, Seoul 02841, Korea

Younghak Kim
Department of Bio-Convergence Engineering, Korea University, Seoul 02841, Korea

Kyeong Min Kim
Division of Medical Radiation Equipment, Korea Institute of Radiologic and Medical Sciences, Seoul 01812, Korea

Wonho Lee*
School of Health and Environmental Science, Korea University, Seoul 02841, Korea

(Received 1 February 2018, in final form 2 April 2018)

A single-photon-emission computed tomography (SPECT) system with a lanthanum-bromide ($LaBr_3$:Ce) scintillator was proposed and simulated to detect neutron-activated prompt γ-rays from suspicious materials. The optimized parameters of the SPECT system were calculated to achieve the best performance. Under the optimized conditions, energy spectra, spatial images, and elemental ratios were obtained and employed to identify hidden materials. The carbon-to-oxygen ratios of the materials calculated through the simulations were consistent with the corresponding theoretical values while the calculated nitrogen-to-oxygen ratios were slightly different from the corresponding theoretical values. In the proposed system, not only the energy spectrum of each element but also the characteristic intensity ratios obtained using the reconstructed images were used to identify the unknown elements of hidden materials in the three-dimensional spatial domain. These results demonstrate the feasibility of using the SPECT system in field applications.

PACS numbers: 25.85.Ec, 28.20.Cz, 87.57.uh
Keywords: Neutron-activated prompt γ-rays, Single-photon-emission computed tomography, Characteristic elemental intensity ratio
DOI: 10.3938/jkps.73.877

I. INTRODUCTION

Prompt γ-ray neutron activation analysis (PGNAA) has been employed to analyze the elements that make up materials. Since its introduction several decades ago [1–3], it has been employed through various instruments for the detection of illegal explosives and drugs at national borders, airports, and harbors [4–6]. The PGNAA is based on a measurement of the unique energy of γ-rays emitted from an unstable nucleus of a material exposed to neutron irradiation. When an atomic nucleus of the target material is exposed to neutrons, neutron-induced prompt γ-rays are emitted through both thermal capture (n, γ) and inelastic reaction (n, n', γ), as shown in Fig. 1. Different nuclei emit prompt γ-rays with different energies; therefore, the elements contained in the target material can be identified by analyzing the energies of the emitted γ-rays.

Owing to their high-energy resolution, high-purity germanium (HPGe) semiconductor detectors have been utilized for the development of PGNAA detection system. In 2015, Seabury *et al.* developed a portable isotopic neutron spectroscopy (PINS) system consisting of a ^{252}Cf source and a portable deuterium-deuterium (DD) neu-

*E-mail: wonhol@korea.ac.kr; Fax: +82-2-940-2829

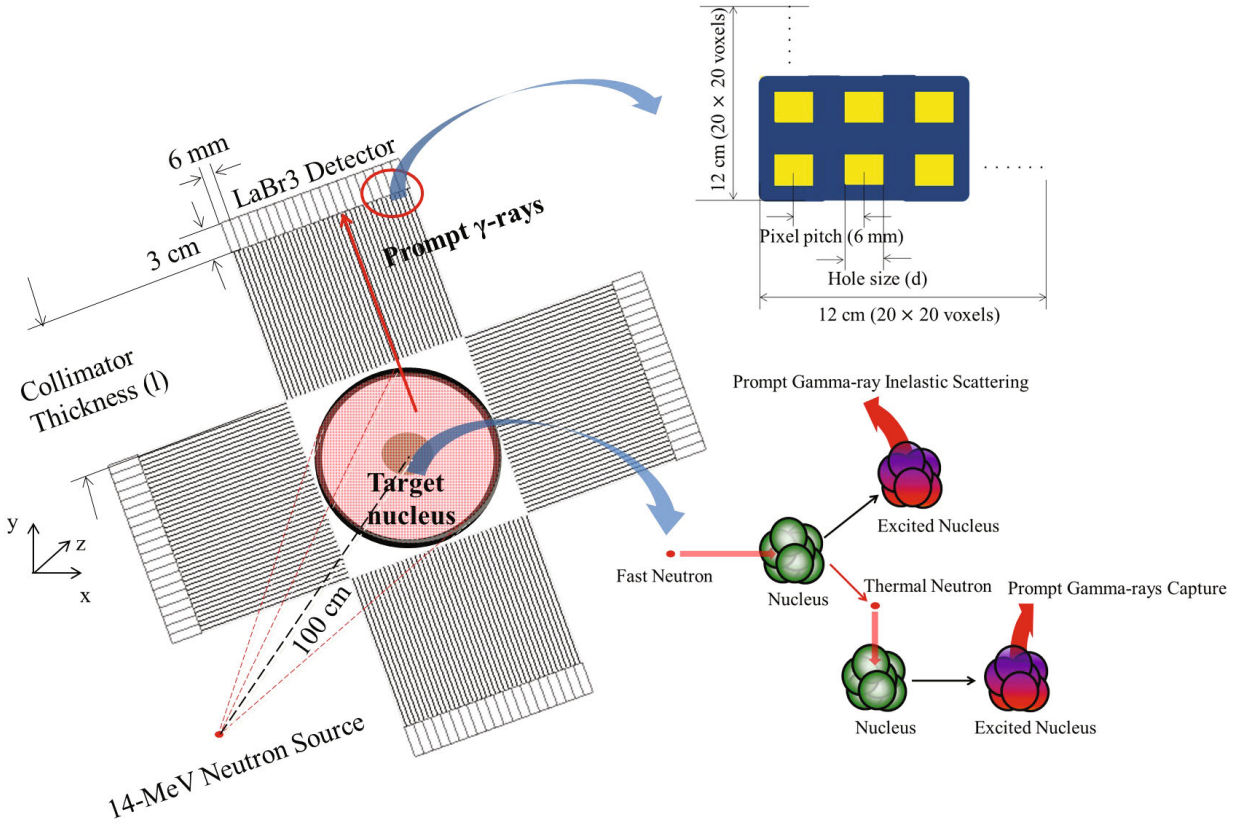

Fig. 1. (Color online) Geometry of the PG-SPECT model employed in the GATE simulation (left) and the principle of the PGNAA (right).

tron generator with an HPGe detector [7]. The prompt γ-rays' peaks in the energy spectrum of a chemical warfare material (CWM) measured using the PINS were compared with those simulated using the MCNP6 code. The results showed that the measured and the simulated prompt γ-rays' peaks were similar to each other. Nicol *et al.* employed the PGNAA detection system with an HPGe detector in measurements at the Nuclear Measurement Laboratory (CEA Cadarache) in 2016 [8]. The measurement identified delayed fission γ-rays from nuclear materials such as ^{235}U and ^{239}Pu. Even though the HPGe semiconductor devices exhibited high spatial and energy resolutions, they could be efficiently utilized only in a small volume ($\sim$ cm^3); in addition, cooling devices were necessary for their operation at room temperature.

For large volumes, lanthanum-halide ($LaBr_3$:Ce and $LaCl_3$:Ce) scintillation detectors, which do not require a cooling equipment, and exhibit improved light output and energy resolution, have been employed in PGNAA [9]. Despite their intrinsic activity (1,436 keV), Naqvi *et al.* demonstrated the superiority of the $LaBr_3$:Ce and $LaCl_3$:Ce γ-ray detectors for the detection of prompt γ-rays in bulk samples with C, O, and H concentrations [10, 11]. In 2013, they employed the $LaBr_3$:Ce detector for the detection of 2.22 (H), 4.43 (C), and 6.13 (O) MeV prompt γ-rays in explosive- and narcotic-like materials exposed to 14-MeV neutrons; their experimental data were in good agreement with the theoretical values [12]. In 2015, T. Lee and W. Lee proposed a multiple-scattering Compton camera (MSCC), which consisted of three $LaBr_3$ detectors, for the detection of 14-MeV neutron-activated prompt γ-rays from explosives and narcotics. The high-energy prompt γ-rays could be imaged using Compton kinematics; the optimized design parameters were calculated [13]. However, if the energy of the source radiation was unknown, more than three detectors were required for image reconstruction. Hence the overall structure of the imaging system became complicated.

In this study, using single-photon-emission computed tomography (SPECT), we investigated the characteristic prompt γ-rays emitted by target materials, such as explosives and narcotics, irradiated with a 14-MeV neutron beam. The characteristic prompt γ-rays emitted from the material were collimated and detected using a two-dimensional (2D) (plane) detector. A shadowgram was constructed using the information measured by the 2D detectors surrounding the material. On the basis of the shadowgram, the three-dimensional (3D) positions of the radiation materials were identified using the SPECT

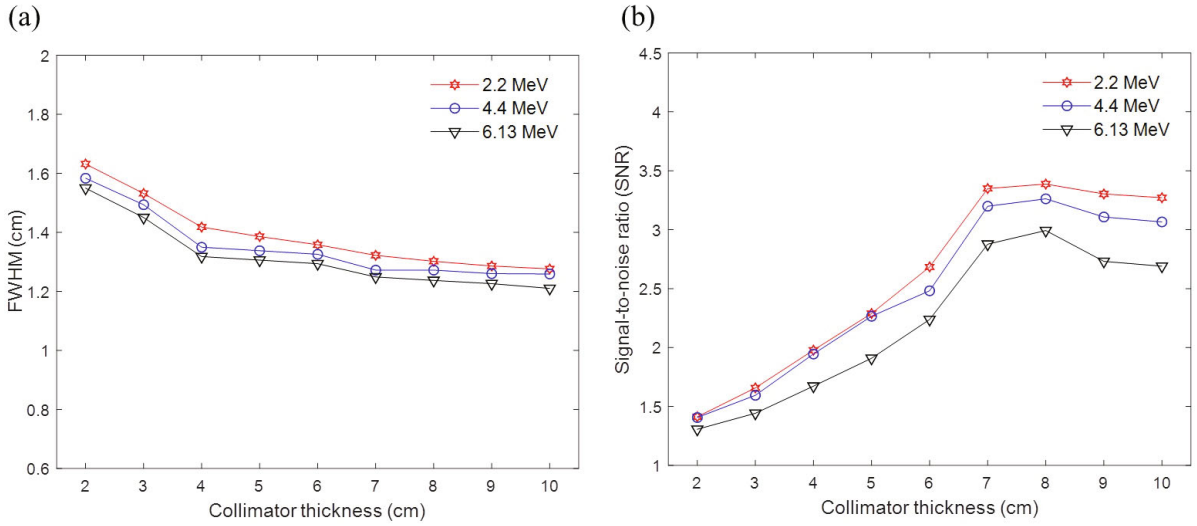

Fig. 2. (Color online) Performance evaluation for various collimator thicknesses and γ-ray energies: (a) resolution (FWHM) and (b) SNR of the reconstructed images.

reconstruction method. The optimized dimensions of the collimation system were calculated, and the performance of the SPECT detection system was evaluated based on the reconstructed images. For identification of the explosive and the narcotic, carbon-to-oxygen (C/O) and nitrogen-to-oxygen (N/O) ratios were calculated using the reconstructed images and the results were compared with theoretical values.

Table 1. Elemental compositions of TNT and cocaine.

Material	Density (g/cm^3)	%H	%C	%N	%O	Elemental ratio	
						C/O	N/O
TNT ($C_3H_5O_6N_3$)	1.63	2.2	37	18.5	42.3	0.9	0.4
Cocaine ($C_{17}H_{21}NO_4$)	0.84	6.9	67.3	4.6	21.1	3.2	0.2

II. MATERIALS AND METHODS

When neutrons undergo an inelastic scattering or are captured in the nuclei of the target material, characteristic prompt γ-rays are emitted from the excited nuclei and can be detected using the SPECT, as shown in Fig. 1. The prompt γ-ray SPECT (PG-SPECT) system consisted of a 14-MeV neutron beam, a cylindrical phantom, and four gantry heads. For the prevention of direct interactions with the neutron beam, each head, composed of a tungsten collimator and $LaBr_3$ detectors, was set perpendicular to the direction between the neutron source and the phantom. A parallel tungsten collimator was employed to selectively pass prompt γ-rays, vertically incident on the detector. The area of each head was 12 cm × 12 cm while the values of the collimator thickness (l) and the hole's size (d) were determined through optimization. The dimensions of each detector module were 12 cm × 12 cm × 3 cm, segmented into 20 × 20 voxels. Each voxel (6 mm × 6 mm × 3 cm) was a single $LaBr_3$ array, attainable by the current technology [14]. The energy resolution of the detector was 5.1% at 511 keV. The centers of the square collimator holes were matched with those of the detector pixels. The distance from the 14-MeV neutron source to the surface of the spherical phantom was 100 cm. The distance from the center of the phantom to each of the heads was 7 cm. The SPECT head was rotated through the whole angular range of 0 - 360° in increments of 5° to detect the prompt γ-rays in every direction. The phantom consisted of a 1-cm spherical target material surrounded by a plastic pipe with a thickness of 1 mm, a diameter of 6 cm, and a length of 12 cm, as shown in Fig. 1. The material between the spherical target and the plastic pipe was air. The target materials were TNT ($C_3H_5O_6N_3$) and cocaine, whose densities were 1.63 g/cm^3 and 0.87 g/cm^3, respectively. Table 1 shows the elemental compositions of the narcotic and the explosive [1]. The hidden materials were irradiated with a neutron flux of 2.0×10^{10} n/cm^2·s, as reported in a previous study [15]. The exposure time was 0.5 s.

The design parameters, such as the collimator thickness and the size of the holes, were optimized based on the quality of the reconstructed images for various prompt γ-rays' energies (2.2, 4.4, and 6.13 MeV). The image resolution and the signal-to-noise ratio (SNR) of the reconstructed images of a γ-ray point-source were employed to determine the quality of the reconstructed images. The image resolution was represented by the

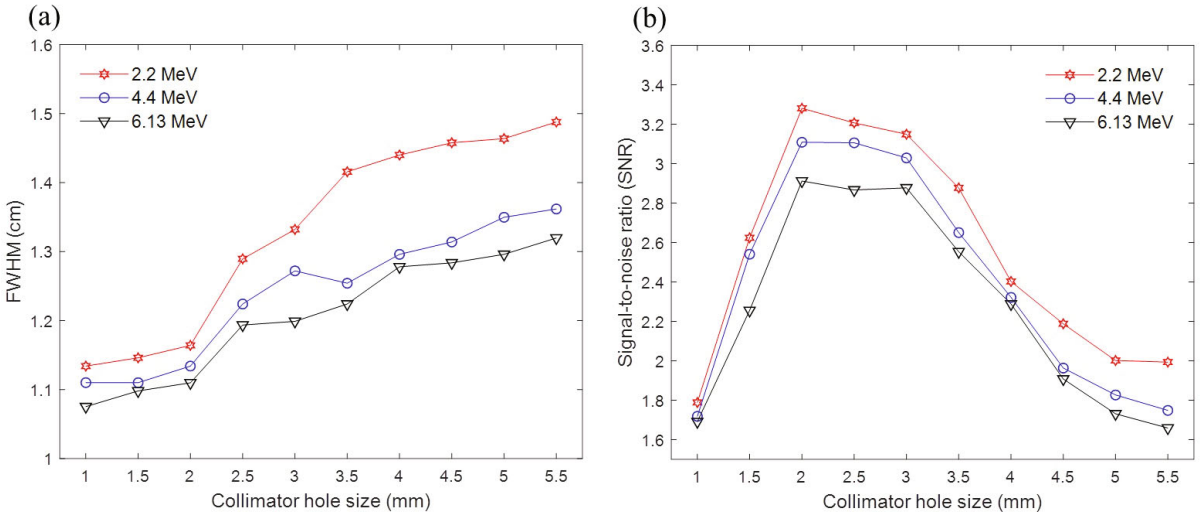

Fig. 3. (Color online) Performance evaluation for various collimator hole's sizes and γ-ray energies: (a) resolution (FWHM) and (b) SNR of the reconstructed images.

full width at half maximum (FWHM) of the γ-ray point-source. The SNR was calculated as

$$\mathrm{SNR} = \frac{\bar{\mu}_{signal}}{\sqrt{\frac{\sum(b_i-\bar{b})^2}{n}}}, \tag{1}$$

where $\bar{\mu}_{signal}$ is the average count in the source pixels within a circle around the maximum-count pixel with a radius equal to the FWHM, b_i and $\bar{b}$ are the counts at pixel i and the average count of the pixels within a circle with the same radius (equal to the value of FWHM) positioned far away from the source region, respectively, and n is the number of image pixels.

Under the optimized conditions, the elemental ratios related to the compositions of the materials were estimated using the intensity ratios observed in the reconstructed image. For estimates of the elemental ratios, not only the different decay rates of the prompt γ-rays for each element but also the energy-dependent response of the detector to γ-rays need to be considered. Therefore, the composition ratio of elements A and B is estimated as [16]

$$\frac{R_A}{R_B} = \frac{\sigma_B(E_n)B_B(E_\gamma)\varepsilon_B(E_\gamma)}{\sigma_A(E_n)B_A(E_\gamma)\varepsilon_A(E_\gamma)} \times \frac{I_A(E_\gamma)}{I_B(E_\gamma)}, \tag{2}$$

where $\sigma(E_n)$ is the neutron absorption cross-section for a neutron energy of E_n (14 MeV) [17], $B(E_\gamma)$ is the branching ratio for the prompt γ-ray with an energy of E_γ [18], $\varepsilon(E_\gamma)$ is the detection efficiency of the $LaBr_3$ detector at E_γ, and $I(E_\gamma)$ is the average image intensity within a circle around the maximum-count pixel with a radius equal to the FWHM at an energy of E_γ.

For the selection of effective events for image reconstruction, $a \pm 2.5\%$ energy window of the total energy deposited in the detectors was employed around each element's peak in the energy spectrum. Images of specific elements were reconstructed using simple back-projections. The simulations were performed using the Geant4 application for tomographic emission (GATE 7.0). The physics of the prompt γ-rays was modeled by applying QGSP_BIC_HP in the Geant4 toolkit. The output data from the GATE simulations were processed using the MATLAB program to select the effective data for the PG-SPECT imaging.

III. RESULTS

1. PG-SPECT design parameters optimization

The collimator thickness, hole size of the detection system, and septal thickness were optimized for several specific prompt γ-ray energies (2.2, 4.4, and 6.13 MeV). In the optimization, the reconstructed images obtained by using the PG-SPECT were evaluated based on the image resolution and the SNR. Figure 2 shows the obtained FWHMs and SNRs of the back-projection images for various collimator thicknesses; the hole size and the pixel pitch of the collimator were set to 3 mm and 6 mm, respectively.

The spatial resolution (FWHM) of the reconstructed point-source did not significantly depend on the incident radiation energy. However, the FWHM improved with increasing of the collimator thickness, as the septal penetration of the γ-rays was inversely proportional to the collimator thickness. The SNR decreased with increasing γ-ray energy, as the amount of septal penetration through the collimator increased. The SNR of the reconstructed image initially improved with increasing collimator thickness. However, after reaching its maximum

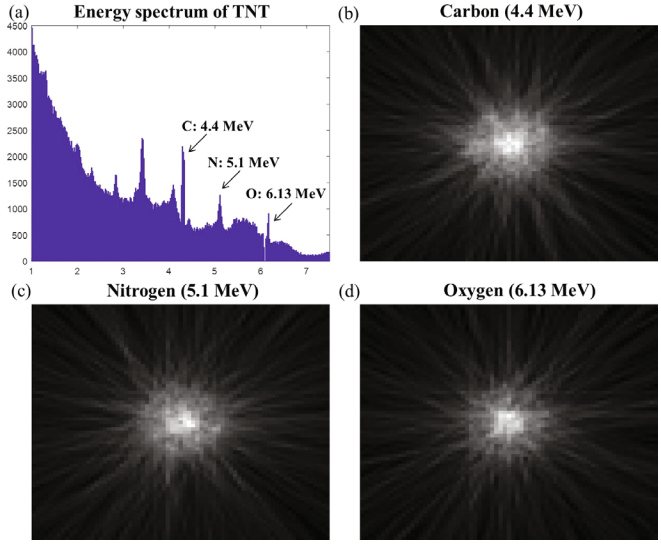

Fig. 4. (Color online) Prompt γ-ray energy spectrum and reconstructed images of the TNT sample. (a) Prompt γ-ray energy spectrum. (b) Carbon (4.4 MeV), (c) nitrogen (5.1 MeV), and (d) oxygen (6.13 MeV) reconstructed images.

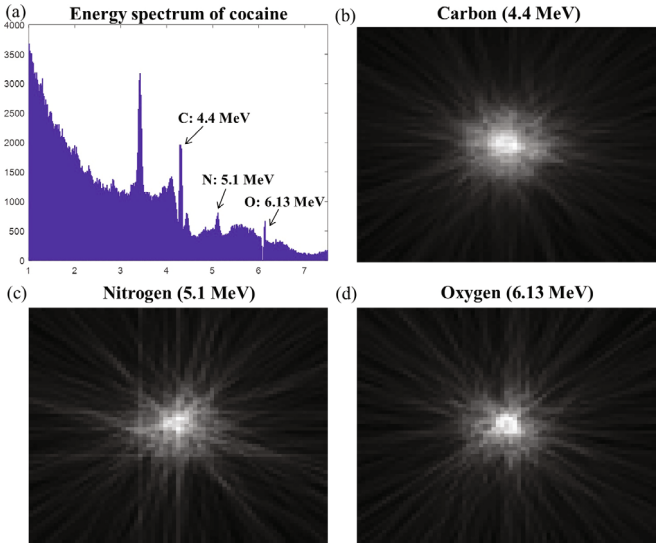

Fig. 5. (Color online) Prompt γ-ray energy spectrum and reconstructed images of the cocaine sample. (a) Prompt γ-ray energy spectrum. (b) Carbon (4.4 MeV), (c) nitrogen (5.1 MeV), and (d) oxygen (6.13 MeV) reconstructed images.

value, the SNR slightly decreased, owing to the septal penetration and number of incident γ-rays (proportional to the SNR), which decreased with increasing collimator thickness. Therefore, the optimal collimator thickness was 7 cm, at which the FWHM was low while the SNR was high.

Figure 3 shows the FWHM and the SNR as functions of the collimator hole's size for the optimal collimator thickness of 7 cm. The FWHM improved with decreasing collimator hole's size. The SNR reached its maximum value when the collimator hole's size was 2 mm. These results indicated that increasing hole's size while maintaining a constant pixel pitch led to an increase in the number of incident γ-rays and a decrease in the septal thickness, which caused septal penetration of γ-rays and degradation of the FWHM. In order to achieve a small FWHM and a high SNR, we set the optimal collimator hole's size to 2 mm. Under the optimized conditions (l = 7 cm, d = 2 mm), the septal thickness was 4 mm. The optimal septal thickness, estimated by using our simulation, was compared with that calculated in Ref. 19. In Ref. 19, the level of septal penetration should be approximately 5%, and the required septal thickness (t) was calculated as

$$t \geq \frac{6d/\mu(E_i)}{l - (3/\mu(E_i))}, \tag{3}$$

where d = 2 mm is the collimator hole's size, l = 7 cm is the thickness of the collimator, and $\mu(E_i)$ is the linear attenuation coefficient (cm^{-1}) of the collimator material at an energy of E_i. The comparison of the acceptable septal thicknesses obtained using a theoretical calculation and our simulation is shown in Table 2, which reveals that the values are similar. Therefore, the optimized collimator's thickness, the hole's size, and the septal thickness were 7 cm, 2 mm, and 4 mm, respectively.

Table 2. Comparison of the acceptable septal thicknesses for various prompt γ-ray energies.

Tungsten density ($\mathrm{g/cm}^3$)	Energy (MeV)	Acceptable septal thickness, from the theoretical calculation (mm)	Optimized septal thickness, from our simulation (mm)
19.3	2.2	4.08	4.0
	4.4	4.81	
	6.13	4.42	

2. Reconstructed images

Figures 4 and 5 show the prompt γ-ray spectra and the reconstructed images for the TNT and the cocaine samples. The intensities of the prompt γ-ray peaks were proportional to the concentrations of the elements in the target materials. All elements observed in the analyzed explosive and narcotic were clearly reconstructed using the data obtained by our detection system. Based on the energy spectrum and the reconstructed images, the major elements of the target materials could be localized and identified.

The TNT and the cocaine samples could be distinguished based on their characteristic C/O and N/O elemental ratios. TNT exhibited small C/O and N/O ratios while cocaine exhibited a high C/O ratio and a small N/O ratio (Table 1). The characteristic elemental ra-

Table 3. Comparison between the theoretical values and the simulation results for the elemental ratios of the analyzed materials.

Material	Theoretical value [1]		Simulation result		Difference (%)	
	C/O	N/O	C/O	N/O	C/O	N/O
TNT	0.9	0.4	0.918	0.43	2.0	7.5
Cocaine	3.2	0.2	3.07	0.217	4.1	8.5

tios were calculated using the intensities observed in the reconstructed image (Table 3, Eq. (2)). The obtained C/O ratios for TNT and cocaine were consistent with the theoretical values. However, as the double escape peak of the 6.13-MeV prompt γ-ray from oxygen significantly overlapped the photoelectric peak of the 5.1-MeV prompt γ-ray from nitrogen, the detection precision of nitrogen could be degraded. Therefore, the double escape peak of the 6.13-MeV prompt γ-ray was subtracted from the photoelectric peak of the 5.1-MeV prompt γ-ray. The obtained N/O ratios for TNT and cocaine differed by 7.5% and 8.5% from the theoretical values, respectively. Consequently, the N/O ratios estimated using our detection system were slightly different from the theoretical values.

IV. CONCLUSION

A SPECT system with optimal collimator parameters was employed to analyze TNT and cocaine samples by measuring prompt γ-rays that they emitted as a result of 14-MeV neutron exposure. The elements of the materials were clearly identified based on the energy spectrum of the detected prompt γ-rays and could be visualized in the 3D spatial domain by using image reconstruction. The theoretical C/O ratios were similar to the ratios obtained by using the intensities observed in the reconstructed images while the theoretical N/O ratios were slightly different from the ratios obtained by using the intensities in the images.

These results demonstrated the feasibility of using the SPECT imaging system for the investigation of suspicious materials. In real applications, the massive shielding material and fixed detector setup can limit the utilization of the proposed system. However, because the system will be used in a fixed position, it can be applied in real conditions as an extended version of the equipment described in Refs. 11 and 12.

ACKNOWLEDGMENTS

This study was supported by the Nuclear Safety Research Program through the Korea Foundation of Nuclear Safety (KoFONS), and through a grant funded by the Nuclear Safety and Security Commission (NSSC), Republic of Korea (1603015) and by a Korea University grant (K1711221).

REFERENCES

[1] D. Strellis and T. Gozani, Appl. Radiat. Isot. **63**, 799 (2005).
[2] B. Perot *et al.*, Appl. Radiat. Isot. **66**, 421 (2008).
[3] I. Jun, W. Kim, M. Smith, I. Mitrofanov and M. Litvak, Nucl. Instr. Meth. A **629**, 140 (2011).
[4] P. Shea, T. Gozani and H. Bozorgmanesh, Nucl. Instr. Meth. A **299**, 444 (1990).
[5] S. Pesente, G. Nebbia, M. Lunardon, G. Viesti, D. Sudac, K. Nad, S. Blagus and V. Valkovic, Nucl. Instr. Meth. A **531**, 657 (2004).
[6] T. Gill Miller, SPIE **2093**, 204 (1994).
[7] E. H. Seabury, C. J. Wharton and A. J. Caffrey, in *IEEE Nuclear science symposium Conference record* (San Diego, CA, United States, October 31-November 7, 2015).
[8] T. Nicol, B. Pérot, C. Carasco, E. Brackx, A. Mariani, C. Passard, E. Mauerhofer and J. Collot, Nucl. Instr. Meth. A **832**, 85 (2016).
[9] A. Favalli, H. C. Mehner, V. Ciriello and B. Pedersen, Appl. Radiat. Isot. **68**, 901 (2010).
[10] A. A. Naqvi, M. S. Al-Anezi, Z. Kalakada, F. A. Al Matouq, M. Maslehuddin, M. A. Gondal, A. A. Isab, K. U. Rehman and M. Dastageer, Appl. Radiat. Isot. **70**, 882 (2012).
[11] A. A. Naqvi, F. A. Al-Matouq, F. Z. Khiari, A. A. Isab, K. U. Rehman and M. Raashid, Nucl. Instr. Meth. A **684**, 82 (2012).
[12] A. A. Naqvi, F. A. Al-Matouq, F. Z. Khiari, A. A. Isab, M. Raashid and K. U. Rehman, Appl. Radiat. Isot. **78**, 145 (2013).
[13] T. Lee and W. Lee, Nucl. Instr. Meth. A **798**, 135 (2015).
[14] A. Kuhn, S. Surti, J. S. Karp, G. Muehllehner, F. M. Newcomer and R. VanBerg, IEEE Trans. Nucl. Sci. **53**, 1090 (2006).
[15] S. Jakhar, C. V. S. Rao, A. Shyam and B. Das, in *IEEE Nuclear science symposium Conference record* (Dresden, Germany, October 19-25, 2008), p. 2335.
[16] C. Carasco, B. Perot, G. Viesti, V. Valkovic, D. Sudac, S. Bernard, A. Mariani, J. L. Szabo, G. Sannie, M. Lunardon, C. Bottosso, S. Moretto, S. Pesente, P. Peerani, V. Sequeira and M. Salvato, Nucl. Instr. Meth. A **582**, 638 (2007).
[17] Available online at: <http://www.tunl.duke.edu/nucldata>.
[18] Available online at: <http://www.intechopen.com/books/gamma-radiation/material-analysis-usingcharacteristic-gamma-rays-induced-by-pulse neutron>.
[19] M. J. Macey, E. J. Grant, J. E. Bayouth, H. B. Giap, S. J. Danna, R. Sirisriro and D. A. Podoloff, Med. Phys. **22**, 1637 (1995).